INSTITUTE OF PHYSICS PUBLISHING JOURNAL OF MICROMECHANICS AND MICROENGINEERING

J. Micromech. Microeng. **17** (2007) 139–146 doi:10.1088/0960-1317/17/1/018

Comments on the size effect on the microcantilever quality factor in free air space

Jiunn-Horng Lee[1,2], Sheng-Ta Lee[3], Chih-Min Yao[2] and Weileun Fang[1,3]

[1] MEMS Institute, National Tsing Hua University, Hsinchu, Taiwan
[2] National Center for High-performance Computing, National Applied Research Laboratories, Hsinchu, Taiwan
[3] Power Mech. Eng. Dept., National Tsing Hua University, Hsinchu, Taiwan

E-mail: fang@pme.nthu.edu.tw

Received 19 August 2006, in final form 15 October 2006
Published 8 December 2006
Online at stacks.iop.org/JMM/17/139

Abstract

This study presents a numerical approach to investigate the size effect on the quality factor associated with the first mode of microcantilever vibration in 1 atm air. The numerical simulation results are verified by experiments and compared with the approximate analytical solutions. Bulk micromachined cantilever arrays are employed as the test vehicles. Based on the experimental and numerical results, this paper proposes a modification to the existing approximate models for air damping analysis by taking into account the geometry effects of the microcantilevers. The arrived semi-empirical equation suggests that the quality factors of the microcantilevers are approximately proportional to $L^{-1.62}$ and $b^{0.62}$ at a low kinetic Reynolds number. Thus, the quality factor of the microcantilever resulting from the free space air can be precisely predicted for design purposes.

(Some figures in this article are in colour only in the electronic version)

1. Introduction

A structure will interact with the surrounding air when operating in an ambient air environment. Due to the scale effect, the air effect on the microelectromechanical systems (MEMS) device cannot be ignored. The hydrodynamic force exerted by air flow induces damping effect on the vibrating microstructure, and further influences the dynamic behavior of the MEMS device. In general, the damping mechanisms for MEMS are classified as squeeze film damping and free space damping. The squeeze film damping has attracted much attention as it occurs in many MEMS devices such as mirrors, switches and resonators. Nevertheless, the free space damping also plays an important role in various MEMS applications. For instance, free vibrating microcantilevers have been widely explored in biosensors [1], chemical sensors [2], accelerometers [3] and scanning probe microscopes (SPMs) [4]. The sensitivity and resolution of the microcantilever devices strongly depend on their quality factors that are closely related to the free space air damping effect. Therefore, it is important to predict the quality factor for the microcantilever design.

It remains a challenging task to derive an exact analytical solution to predict the interaction between the air and microcantilevers. The approximate analytical models have been presented in [5–7]. Most of them are based on the harmonic oscillating sphere theory [8], and model the microcantilevers as a sphere or a string of spheres. These simplified approximate analytical models have been broadly applied to many areas including the development of micro power generator [9, 10], study of air viscous damping effects by a Fabry–Perot micro-opto-mechanical device (FPMOD) [11], absolute pressure measurement [12], mass sensing resonators [13], measurement of liquid viscosity and density [14] and design of atomic force microscopy probes [15]. However, the geometry of the sphere-related models and the microcantilevers is different intrinsically. The validity of these simplified models needs to be further investigated. On

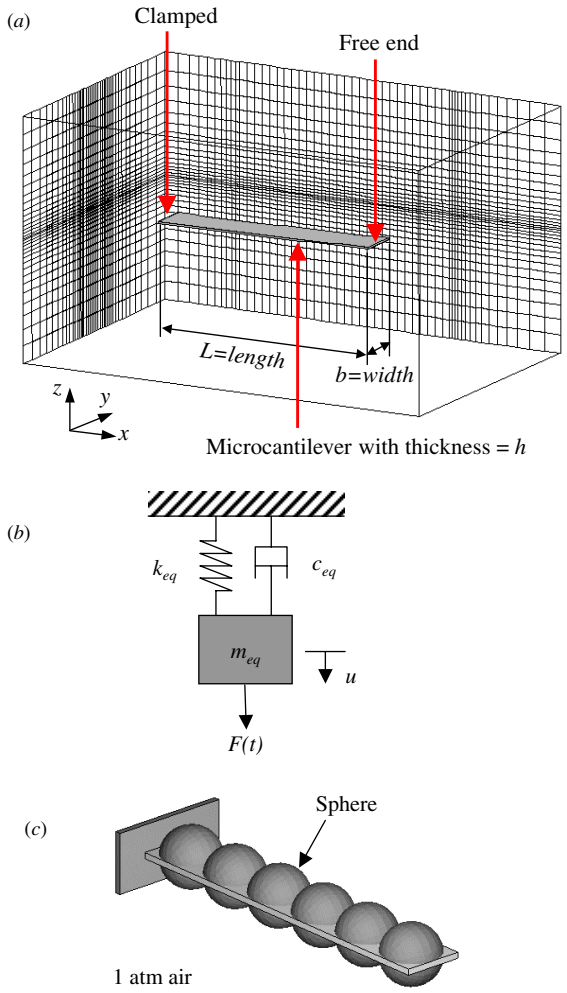

Figure 1. Schematic illustrations of (*a*) the numerical model of the cantilever beam vibrating in an ambient air environment, (*b*) an equivalent damped SDOF system and (*c*) Bead model of the microcantilever.

the other hand, the numerical simulation of fluid-structure interaction (FSI) has been extensively employed in the macro world [16], and has been successfully applied to some MEMS applications [17, 18] as well. The numerical calculation that minimizes the approximations could not only simulate the dynamic behavior of the microcantilevers more accurately but also provide more insight into the problem of structure–fluid interaction through scientific visualization. Thus, more innovative designs of micro structures can be inspired.

This study presents a numerical approach, as shown in figure 1(*a*), that exploits the FSI simulation to investigate the size effect on quality factor associated with the first mode of microcantilever vibrating in 1 atm air. The numerical simulation results are verified by experiments and compared with the approximate analytical solutions. Moreover, based on the experimental and numerical results, this paper proposes a semi-empirical expression to estimate the quality factors of the microcantilevers for engineering design purpose. In application, the thermal oxide microcantilever arrays with various dimensions were fabricated and characterized.

2. Modeling and analysis

There are various existing theoretical analyses that have been reported to study the air damping of a vibrating microcantilever [5, 7]. As a comparison, this study employs the numerical approach to investigate the dynamics of a microcantilever under the influence of ambient air.

2.1. The existing theoretical analyses

As indicated in figure 1(*a*), the discussed vibrating microcantilever has a length L, width b and thickness h. In general, the hydrodynamic force induced by ambient air will introduce added mass and added damping effects on the vibrating microcantilever [8, 19]. The added mass that is much smaller than the mass of cantilever beam is ignored in this study. Thus, the dynamic characteristic of the microcantilever vibrating at its fundamental mode can be modeled as a damped spring–mass system [4, 20], as shown in figure 1(*b*). The added damping effect exerted on the cantilever beam is approximated by an equivalent damping coefficient c_{eq}. The equation of motion of this damped single-degree-of-freedom (SDOF) system shown in figure 1(*b*) is

$$m_{\mathrm{eq}}\ddot{u} + c_{\mathrm{eq}}\dot{u} + k_{\mathrm{eq}}u = F(t) \tag{1}$$

in which $k_{\mathrm{eq}} = Ebh^3/(4L^3)$ is the equivalent stiffness, $m_{\mathrm{eq}} = 0.24\rho_b hbL$ is the equivalent mass and the undamped natural frequency ω_n is

$$\omega_n = \sqrt{\frac{k_{\mathrm{eq}}}{m_{\mathrm{eq}}}} = 3.52\frac{h}{L^2}\sqrt{\frac{E}{12\rho_b}}, \tag{2}$$

where $F(t)$, u, E and ρ_b are the external force, displacement of the tip, Young's modulus and density of the cantilever beam, respectively. Equation (1) can be rewritten as [20]

$$\ddot{u} + 2\zeta\omega_n\dot{u} + \omega_n^2 u = \frac{1}{m_{\mathrm{eq}}}F(t), \tag{3}$$

where $\zeta = c_{\mathrm{eq}}/c_{\mathrm{cr}}$ is the damping ratio and $c_{\mathrm{cr}} = 2m_{\mathrm{eq}}\omega_n$ is the critical damping. The quality factor Q of the cantilever beam is then defined as [20]

$$Q = \frac{1}{2\zeta} = \frac{m_{\mathrm{eq}}\omega_n}{c_{\mathrm{eq}}}. \tag{4}$$

Thus, the quality factor Q can be determined by the bandwidth of the frequency response or by the exponential decay of vibration amplitude [20].

Due to the complicated dynamics between the coupling of structure and air, it is still a challenge to establish the analytical model to predict the quality factor of micromachined structures. Some simplified analytical approaches have been reported to estimate the quality factor instead. For example, Newell [5] has applied Stokes' law to yield the quality factor, as pointed out in equation (5)

$$Q_{\mathrm{Newell}} = \frac{1}{24}\frac{bh^2}{L^2}\frac{\sqrt{E\rho_b}}{\mu}, \tag{5}$$

where μ is the viscosity of air. Hosaka and Itao [7] have employed a bead model shown in figure 1(*c*) to represent the cantilever beam as a string of spheres. The damping ratio is

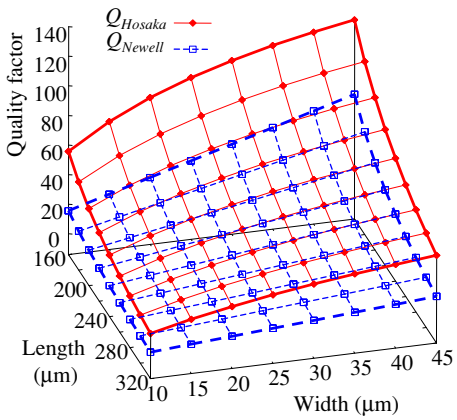

Figure 2. The microcantilever quality factor predicted by Newell (Q_{Newell}) and Hosaka (Q_{Hosaka}) for different beam widths and lengths.

thus approximated by including the effect of flow interaction among spheres, and can be expressed as

$$\zeta_{\text{Hosaka}} = \frac{3\pi\mu b + \frac{3}{4}\pi b^2\sqrt{2\rho_a\mu\omega}}{4\rho_b h b^2\omega_n}, \tag{6}$$

where ρ_a and ω represent the density of air and the oscillating frequency of the cantilever beam, respectively. Thus, the quality factor of the cantilever beam vibrating in its first mode is

$$Q_{\text{Hosaka}} = \frac{1}{2\zeta_{\text{Hosaka}}} = \frac{2\rho_b h b^2\omega_n}{3\pi\mu b + \frac{3}{4}\pi b^2\sqrt{2\rho_a\mu\omega}}. \tag{7}$$

As the kinetic Reynolds number $R_k = \rho_a\omega b^2/4\mu$ is small, the second term in the denominator of equation (7) is smaller than that of the first term, hence, equation (7) can be rewritten as

$$Q'_{\text{Hosaka}} = \frac{2\rho_b h b^2\omega_n}{3\pi\mu b} = 0.22\frac{bh^2}{L^2}\frac{\sqrt{E\rho_b}}{\mu} \tag{8}$$

which has a similar form as Q_{Newell}.

Figure 2 shows the microcantilever quality factor predicted by Newell (Q_{Newell}) and Hosaka (Q_{Hosaka}) for different beam widths and lengths. The scaling analysis on equations (1) and (2) indicates that the equivalent mass m_{eq} is proportional to (Lhb) and the resonant frequency ω_n is proportional to (h/L^2). According to the scaling analysis on equations (5) and (8), the quality factors of Q_{Newell} and Q'_{Hosaka} are proportional to $(bh^2)/L^2$. Consequently, the equivalent damping coefficient c_{eq} only varies with (L^1) due to the scaling analysis on equation (4). In short, c_{eq} is proportional to (L^1) and (b^0) based on the model of [5] and [7]. However, the equivalent viscous damping coefficient c_{eq} should increase as the width of the cantilever beam increases because the drag force exerted on the cantilever beam is increased as the frontal area of the cantilever beam increases [21]. Thus, this study employs the numerical simulation to discuss the validity of the simplified model of [5] and [7].

2.2. The present numerical simulation

The study employed the CFD-ACE+ commercial software to simulate the dynamic behavior of SiO_2 microcantilevers. The FSI function was applied to simulate the free vibration of the SiO_2 microcantilever immersed in an ambient air environment.

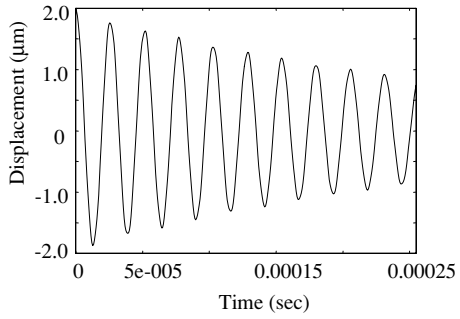

Figure 3. Displacement-time history of the free end predicted from numerical simulation.

Thus, the damping ratio as well as the quality factor can be determined from the exponential decay of vibration amplitude [20]. The CFD-ACE+ iteratively calculated between a fluid solver that uses finite volume method (FVM) for Navier–Stokes equations and a structure solver that uses finite element method (FEM) for solid mechanics to solve the multiphysics coupling problem.

The numerical FSI simulation model is shown in figure 1(*a*). Because of the high aspect ratio (length/thickness) of the thin film structure, the solid-shell element is used to model the microcantilever. The Young's modulus and density of the SiO_2 microcantilever, which were measured by resonance test, are $E = 73.38$ GPa and $\rho_b = 2.49 \times 10^{-15}$ kg μm^{-3}. The density and viscosity of the air are $\rho_a = 1.20$ kg m^{-3} and $\mu = 1.85 \times 10^{-5}$ kg (m s)$^{-1}$, respectively. The ambient air pressure is 1 atm. To simulate the free vibration of the cantilever beam, an end-load was specified to give a 2 μm out-of-plane tip deflection as the initial condition. A transient vibration was simulated by the software after the initial tip deflection of the cantilever was released. Figure 3 shows a typical simulated displacement-time history of the free end. The damping ratio ζ can be obtained after curve fitting of the simulation results in figure 3 to the exponential decay curve. The quality factor of the cantilever beam can be further determined by equation (4).

3. Experiments

Bulk micromachined SiO_2 cantilever beams were employed as the test structures for experiment. The quality factors of the microcantilevers were determined from the measured frequency responses of the test structures. The SiO_2 cantilever beams were excited by a PZT transducer and characterized using a laser Doppler vibrometer (LDV) system together with a dynamic signal analyzer.

In this experiment, the SiO_2 microcantilevers were fabricated by bulk micromachining. The fabrication process flow is illustrated in figure 4. The (1 0 0) single crystal silicon substrate was first placed in a furnace to grow a 1.15 μm thick thermal oxide film at 1050 °C, as shown in figure 4(*a*). After the photolithography, the thermal oxide was patterned by reactive ion etching (RIE), as shown in figure 4(*b*). Finally, the silicon substrate was wet etched anisotropically using tetramethyl ammonium hydroxide (TMAH) etchant. As shown in figure 4(*c*), the SiO_2 microcantilevers were freely suspended on the substrate after bulk silicon etching.

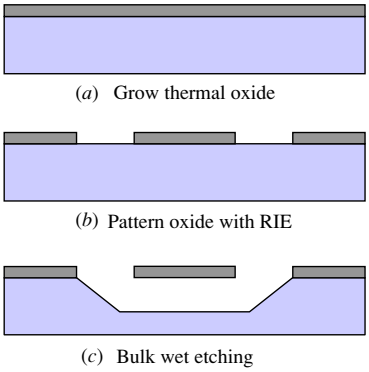

Figure 4. Fabrication process flow for the test microcantilever array.

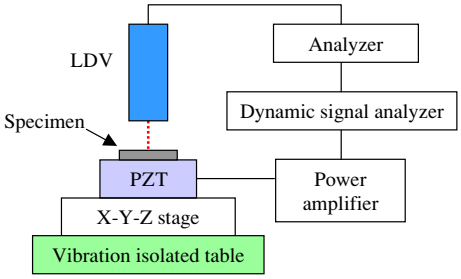

Figure 5. Experiment setup to measure the dynamic response of the microcantilever.

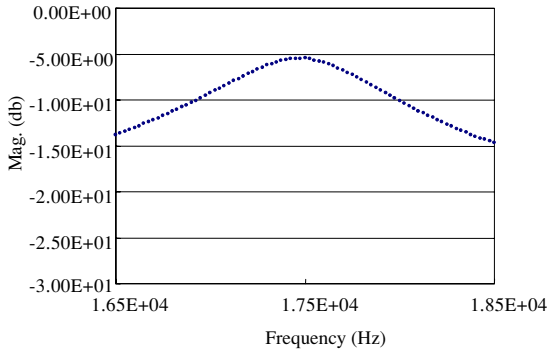

Figure 6. Typical measured frequency response of a microcantilever.

The experimental setup is shown in figure 5. The specimen was attached to a PZT transducer. The dynamic signal analyzer (HP 35670A) generated harmonic signal through the power amplifier to drive the PZT transducer to excite the cantilever beams. The LDV system (Graphtec AT-3500) measured the dynamic response at each microcantilever tip, and the measured signal was analyzed by the dynamic signal analyzer. Figure 6 shows one of the typical measured frequency responses of the microcantilevers from the dynamic signal analyzer. The Lorentzian curve fitting for the frequency responses with equation (9) [22] was performed to extract the quality factors of the microcantilevers,

$$\text{Frequency response function} = \frac{D_0(\omega_n/\omega)}{\sqrt{1+Q^2(\omega/\omega_n-\omega_n/\omega)^2}}, \tag{9}$$

where D_0 is a constant.

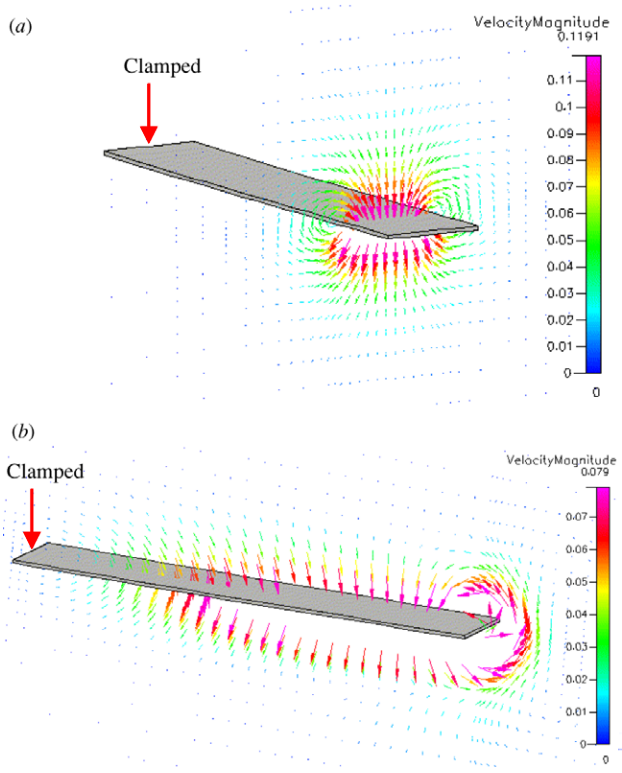

Figure 7. The predicted velocity field of air flow (*a*) along the beam width and (*b*) along the beam length.

4. Results and discussion

The typical simulation results are shown in figure 7. Figure 7(*a*) shows the simulated velocity field of air flow distributed in a particular y–z plane (i.e. along the beam width). Figure 7(*b*) shows the velocity field of air flow distributed in a particular x–z plane (i.e. along the beam length). Table 1 lists the quality factors of the microcantilevers determined from the experiments. The microcantilevers have length ranging from 160 μm to 320 μm and width ranging from 10 μm to 45 μm. The comparison of the measured quality factor Q_{exp} with the predicted results from Newell Q_{Newell}, Hosaka Q_{Hosaka} and numerical simulation Q_{sim}, respectively are shown in both figures 8(*a*)–(*c*) and table 2. Figure 8(*c*) shows that the numerical simulation results agree well with the experimental results, whereas, figures 8(*a*), (*b*) show that the analytical results of Q_{Newell} and Q_{Hosaka} have significant deviation from the experiment ones at some particular dimensions of microcantilevers.

As shown in equation (5), the quality factor Q_{Newell} is linearly proportional to the width b of a microcantilever. According to equation (7), the quality factor Q_{Hosaka} becomes approximately linearly proportional to the width b at low R_k. However, it is clearly shown in figure 8 that Q_{exp} is not linearly proportional to the width of the cantilever beam. As a comparison, a surface fitting was applied to the experimental results to determine the relationship between the quality factor and the in-plane dimensions of the microcantilever. This study proposes an improvement over the bead model shown

Table 1. Measured quality factors Q_{exp} for the test microcantilever array.

$L\backslash b$	10	15	20	25	30	35	40	45
160	32.45	38.62	42.29	46.30	48.54	50.28	51.34	52.31
180	27.41	33.52	36.44	40.18	41.76	43.82	44.68	45.54
200	23.92	28.60	31.24	34.76	36.51	38.12	39.20	40.56
220	20.67	25.25	28.14	30.69	32.34	33.66	35.00	36.28
240	18.37	22.52	25.34	27.29	29.28	30.77	31.60	32.90
260	16.18	19.90	23.10	24.97	26.16	27.81	28.96	29.84
280	14.79	17.84	20.54	22.63	23.94	25.19	26.29	27.70
300	13.11	16.47	18.63	20.32	21.93	22.91	23.81	24.67
320	12.16	15.08	17.19	18.77	20.32	21.14	22.23	23.26

b = width, L = length, unit = μm.

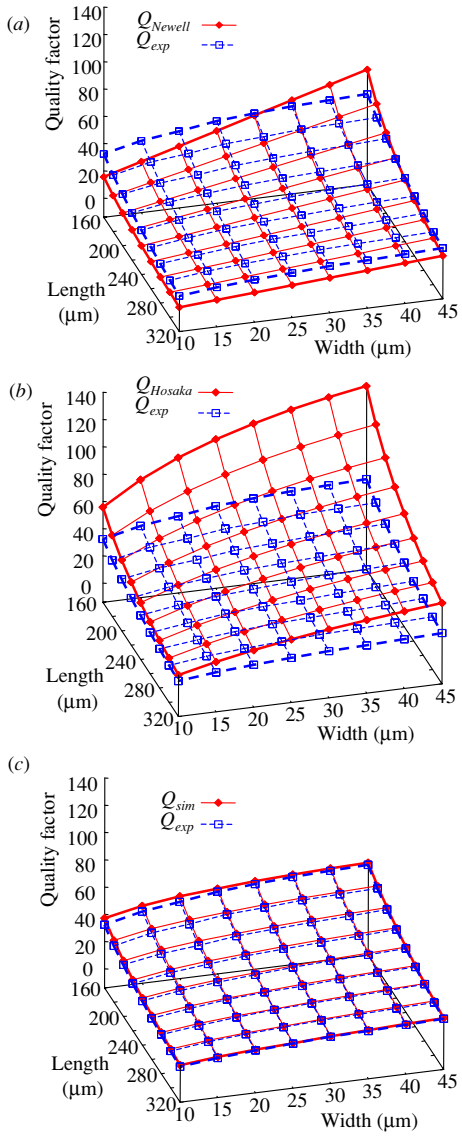

Figure 8. Comparison of predicted and measured quality factors, (*a*) Q_{Newell} versus Q_{exp}, (*b*) Q_{Hosaka} versus Q_{exp} and (*c*) Q_{sim} versus Q_{exp}.

in figure 1(*c*) [7] by incorporating some geometry effects of the microcantilever. Thus, the equivalent damping coefficient established in this study has the form

$$(c_{\text{eq}})_{\text{Lee}} = \left(A_1(3\pi\mu b) + A_2\left(\frac{3}{4}\pi b^2\sqrt{2\rho_a\mu\omega}\right)\right) \times \left(\frac{L}{b}\right)\left(\frac{b}{L}\right)^{A_3}, \tag{10}$$

where A_1, A_2 and A_3 are constants, A_1 is the geometry factor for Stokes drag force from a sphere to a square plate, A_2 is the geometry factor for Basset history force from a sphere to a square plate, $\frac{L}{b}$ is the no. of sphere in the cantilever beam, $\left(\frac{b}{L}\right)^{A_3} = G_{\text{eff}}$ is the geometry effective factor of the cantilever beam.

Substituting equation (10) into equation (4), the expression of the quality factor becomes

$$Q_{\text{Lee}} = \frac{(0.24\rho_b hbL)\omega_n}{\left(A_1(3\pi\mu b) + A_2\left(\frac{3}{4}\pi b^2\sqrt{2\rho_a\mu\omega}\right)\right)\left(\frac{L}{b}\right)\left(\frac{b}{L}\right)^{A_3}}. \tag{11}$$

The geometry factors were determined to be $A_1 = 0.69$, $A_2 = 0.33$ and $A_3 = 0.38$ after surface fitting of equation (11) to the measurement results in figure 8. Therefore,

$$Q_{\text{Lee}} = \frac{(0.24\rho_b hbL)\omega_n}{\left(0.69(3\pi\mu b) + 0.33\left(\frac{3}{4}\pi b^2\sqrt{2\rho_a\mu\omega}\right)\right)\left(\frac{L}{b}\right)\left(\frac{b}{L}\right)^{0.38}}. \tag{12}$$

Note that equation (12) is a semi-empirical expression yielded from experiment over the measurement range of $0.10 < R_k < 10.60$. The variations of the quality factors Q_{Lee} and Q_{exp} are less than 3.33%, as shown in figure 9. If the A_2 term in equation (10) is ignored at low R_k, the present equivalent damping coefficient $(c_{\text{eq}})_{\text{Lee}}$ of the microcantilever is proportional to $L^{0.62}$ and $b^{0.38}$, and the quality factor Q_{Lee} of the cantilever beam is proportional to $(b^{0.62}h^2)/L^{1.62}$. As a comparison, the equivalent damping coefficient c_{eq} in [5] and [7] is proportional to (L^1) and (b^0), and the quality factors of Q_{Newell} and Q'_{Hosaka} are proportional to $(bh^2)/L^2$. In conclusion, the approximate analytical models of [5] and [7] overestimate the beam length effect on air damping but underestimate the beam width effect on air damping. The geometry effective factor G_{eff} that is proportional to $(b/L)^{0.38}$ plays an important role in this regard. As the beam width b increases or beam length L decreases, the influence of the A_2 term in denominator needs to be taken into consideration. In

Table 2. Comparison of measured quality factors Q_{exp} with analytical results (Q_{Newell}, Q_{Hosaka}) and numerical simulation results (Q_{sim}).

	10			15			20			25			30			35			40			45		
	Error (%)			Error (%)			Error (%)			Error (%)			Error (%)			Error (%)			Error (%)			Error (%)		
$L\backslash b$	EQ_N	EQ_H	EQ_S	EQ_N	EQ_H	EQ_S	EQ_N	EQ_H	EQ_S	EQ_N	EQ_H	EQ_S	EQ_N	EQ_H	EQ_S	EQ_N	EQ_H	EQ_S	EQ_N	EQ_H	EQ_S	EQ_N	EQ_H	EQ_S
160	−51.86	71.93	14.7	−39.31	87.70	11.1	−26.11	101.56	9.7	−15.64	105.83	5.1	−3.44	113.08	4.4	8.77	119.07	3.6	21.74	125.54	3.5	34.41	130.53	3.1
180	−54.94	66.55	14.7	−44.75	78.85	9.0	−32.24	95.06	9.2	−23.20	99.08	4.3	−11.30	109.00	5.2	−1.39	113.05	3.5	10.52	120.48	4.0	22.00	126.02	3.9
200	−58.19	59.11	12.8	−47.55	76.36	10.5	−35.98	92.83	10.7	−28.08	96.17	5.3	−17.83	104.79	5.5	−8.18	110.65	4.7	2.04	116.86	4.8	10.95	119.63	3.5
220	−60.04	55.88	13.4	−50.89	70.53	9.5	−41.26	83.90	8.0	−32.68	91.85	5.1	−23.35	100.49	5.6	−14.05	107.66	5.5	−5.54	112.09	4.7	2.51	114.99	3.5
240	−62.22	50.52	12.1	−53.73	65.19	8.4	−45.19	77.43	6.4	−36.39	88.35	5.2	−28.86	94.09	4.2	−20.99	99.74	3.4	−12.09	107.15	4.3	−5.02	109.60	3.0
260	−63.41	48.21	12.7	−55.38	63.17	9.2	−48.79	70.74	4.3	−40.77	81.34	3.0	−32.15	92.05	5.0	−25.53	96.01	3.3	−18.27	101.00	3.0	−10.76	105.97	3.0
280	−65.52	41.99	10.1	−57.12	60.26	9.2	−50.34	69.91	5.4	−43.61	77.73	2.4	−36.05	87.01	3.9	−29.10	93.37	3.7	−22.37	98.36	3.4	−17.11	99.21	1.4
300	−66.13	41.50	11.5	−59.50	54.04	6.6	−52.28	66.94	5.0	−45.32	77.02	3.2	−39.22	83.13	3.2	−32.08	91.23	4.1	−25.33	97.44	4.5	−18.93	102.03	4.4
320	−67.85	35.69	8.6	−61.14	50.40	5.4	−54.57	62.30	3.3	−47.95	72.46	1.5	−42.32	78.35	1.9	−35.34	87.46	3.5	−29.73	91.72	3.0	−24.42	94.63	2.1

EQ_N = error of Q_{Newell}, EQ_H = error of Q_{Hosaka}, EQ_S = error of Q_{sim}.

Table 3. Comparison of predicted and measured quality factors Q_{Lee} and Q_{exp} for a new microcantilever family.

L (μm)	142	162	182	202	222	242	262	282	302
Q_{Lee}	39.37	33.28	28.60	24.90	21.93	19.49	17.47	15.77	14.32
Q_{exp}	39.26	32.49	28.16	25.19	22.35	20.04	17.67	15.86	14.62
Error (%)	0.28	2.43	1.55	−1.14	−1.88	−2.72	−1.12	−0.57	−2.04

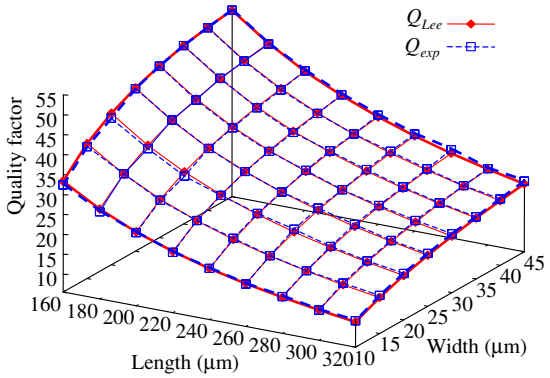

Figure 9. Variation of quality factors Q_{Lee} and Q_{exp} with the width and length of the microcantilever.

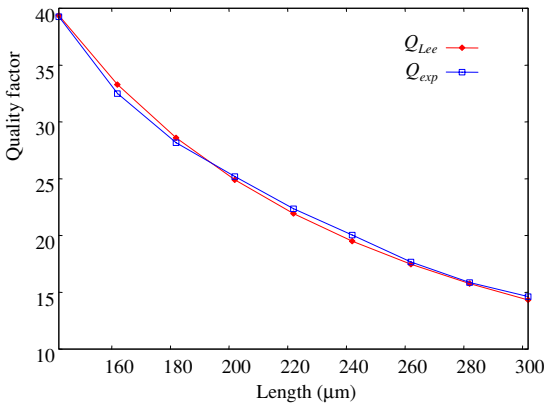

Figure 10. Comparison of predicted and measured quality factors Q_{Lee} and Q_{exp} for a new microcantilever family.

other words, the quality factor Q_{Lee} is no longer simplified to be proportional to $(b^{0.62}h^2)/L^{1.62}$ as R_k increases.

To demonstrate the validity of equation (12), the SiO_2 microcantilever array, with thickness $h = 0.97$ μm, width $b = 25$ μm and length L ranging from 142 μm to 302 μm, were fabricated and characterized. Figure 10 and table 3 show the quality factors of the microcantilevers determined from the experiments, and predicted by equation (12) as well. It indicates that the results predicted by equation (12) have only less than 3% deviation with the measurements. In summary, equation (12) can be employed to accurately predict the quality factor of microcantilevers.

5. Conclusions

The size effect on the first mode quality factors of microcantilevers in free air space has been investigated by experiments and numerical simulations. The experiments extracted the quality factors by measuring the dynamic frequency responses of the microcantilevers. The numerical simulations determine the quality factors using the free vibration model of the microcantilevers. The numerical simulation results are in good agreement with the experimental results. In addition, the velocity field of air flow is available from the simulation. It provides valuable information while designing the micromachined structures. In summary, the numerical FSI computation is a promising method to predict the dynamic characteristics of microstructures in an ambient air environment. Based on the experimental and numerical results, this study has also modified the existing approximate models for air damping analysis by taking into account the geometry effects of the microcantilevers. The quality factors of the microcantilevers are approximately proportional to $L^{-1.62}$ and $b^{0.62}$ at low R_k. Thus, the air damping and quality factor of microcantilever can be precisely predicted by the proposed semi-empirical expression for design purpose. However, the physical meaning of these factors and the full applicable range of the semi-empirical equation need to be further investigated.

Acknowledgments

This research is based on work supported by the National Science Council of Taiwan under grant of NSC-94-2212-E-007-026. The authors would like to thank the Central Regional MEMS Research Center of the National Science Council, the Semiconductor Research Center of the National Chiao Tung University and the National Nano Device Laboratory of NSC for providing the fabrication facilities.

References

[1] Ziegler C 2004 Cantilever-based biosensors *Anal. Bioanal. Chem.* **379** 946–59
[2] Lavrik N V, Sepaniak M J and Datskos P G 2004 Cantilever transducers as a platform for chemical and biological sensors *Rev. Sci. Instrum.* **75** 2229–53
[3] Brandl M and Kempe V 2001 High performance accelerometer based on CMOS technologies with low cost add-ons *IEEE MEMS 2001 (Interlaken, Switzerland)* pp 6–9
[4] Chen G Y, Warmack R J, Thundat T, Allison D P and Huang A 1994 Resonance response of scanning force microscopy cantilevers *Rev. Sci. Instrum.* **65** 2532–7
[5] Newell W E 1968 Miniaturization of tuning forks *Science* **161** 1320–6
[6] Blom F R, Bouwstra S, Elwenspoek M and Fluitman J H J 1992 Dependence of the quality factor of micromachined silicon beam resonators on pressure and geometry *J. Vacuum Sci. Technol.* B **10** 19–26
[7] Hosaka H and Itao K 1999 Theoretical and experimental study on airflow damping of vibrating microcantilevers *Trans. ASME. J. Vib. Acoust.* **121** 64–9
[8] Landau L D and Lifshitz E M 1987 *Fluid Mechanics* 2nd edn (New York, NY: Pergamon)

[9] Mizuno M and G Chetwynd D 2003 Investigation of a resonance microgenerator *J. Micromech. Microeng.* **13** 209–16
[10] Kulah H and Najafi K 2004 An electromagnetic micro power generator for low-frequency environmental vibrations *IEEE MEMS 2004 (Maastricht, Netherlands)* pp 237–40
[11] Nieva P M, McGruer N E and Adams G G 2006 Air viscous damping effects in vibrating microbeams *Proc. SPIE* **6169** 148–59
[12] Bianco S *et al* 2006 Silicon resonant microcantilevers for absolute pressure measurement *J. Vac. Sci. Technol.* B **24** 1803–9
[13] Vignola J F, Judge J A, Jarzynski J, Zalalutdinov M, Houston B H and Baldwin J W 2006 Effect of viscous loss on mechanical resonators designed for mass detection *Appl. Phys. Lett.* **88** 041921
[14] Shih W Y, Li X, Gu H, Shih W-H and Aksay I A 2001 Simultaneous liquid viscosity and density determination with piezoelectric unimorph cantilevers *J. Appl. Phys.* **89** 1497–505
[15] Walters D A, Cleveland J P, Thomson N H, Hansma P K, Wendman M A, Gurley G and Elings V 1996 Short cantilevers for atomic force microscopy *Rev. Sci. Instrum.* **67** 3583–90
[16] Bathe K J and Zhang H 2004 Finite element developments for general fluid flows with structural interactions *Int. J. Numer. Methods Eng.* **60** 213–32
[17] Athavale M M, Yang H Q and Przekwas A 1999 Coupled fluid-thermal-structure simulations in microvalves and microchannels *Proc. MSM'99 (San Juan, Puerto Rico)* pp 570–3
[18] Giridharan M G, Stout P, Yang H Q, Athavale M, Dionne P and Przekwas A 2001 Multi-disciplinary CAD system for MEMS *J. Model. Simul. Microsyst.* **2** 43–50
[19] Hosaka H, Itao K and Kuroda S 1995 Damping characteristics of beam-shaped micro-oscillators *Sensors Actuators* A **49** 87–95
[20] Thomson W T 1993 *Theory of Vibration with Applications* 4th edn (Englewood Cliffs, NJ: Prentice Hall)
[21] White F M 2002 *Fluid Mechanics* 5th edn (New York, NY: McGraw-Hill)
[22] Patil S and Dharmadhikari C V 2002 Investigation of the electrostatic forces in scanning probe microscopy at low bias voltages *Surf. Interface Anal.* **33** 155–8